



Universiteit  
Leiden

The Netherlands

## Evolutionary adaptability of $\beta$ -lactamase: a study of inhibitor susceptibility in various model systems

Alen, I. van

### Citation

Alen, I. van. (2023, September 20). *Evolutionary adaptability of  $\beta$ -lactamase: a study of inhibitor susceptibility in various model systems*. Retrieved from <https://hdl.handle.net/1887/3641470>

Version: Publisher's Version

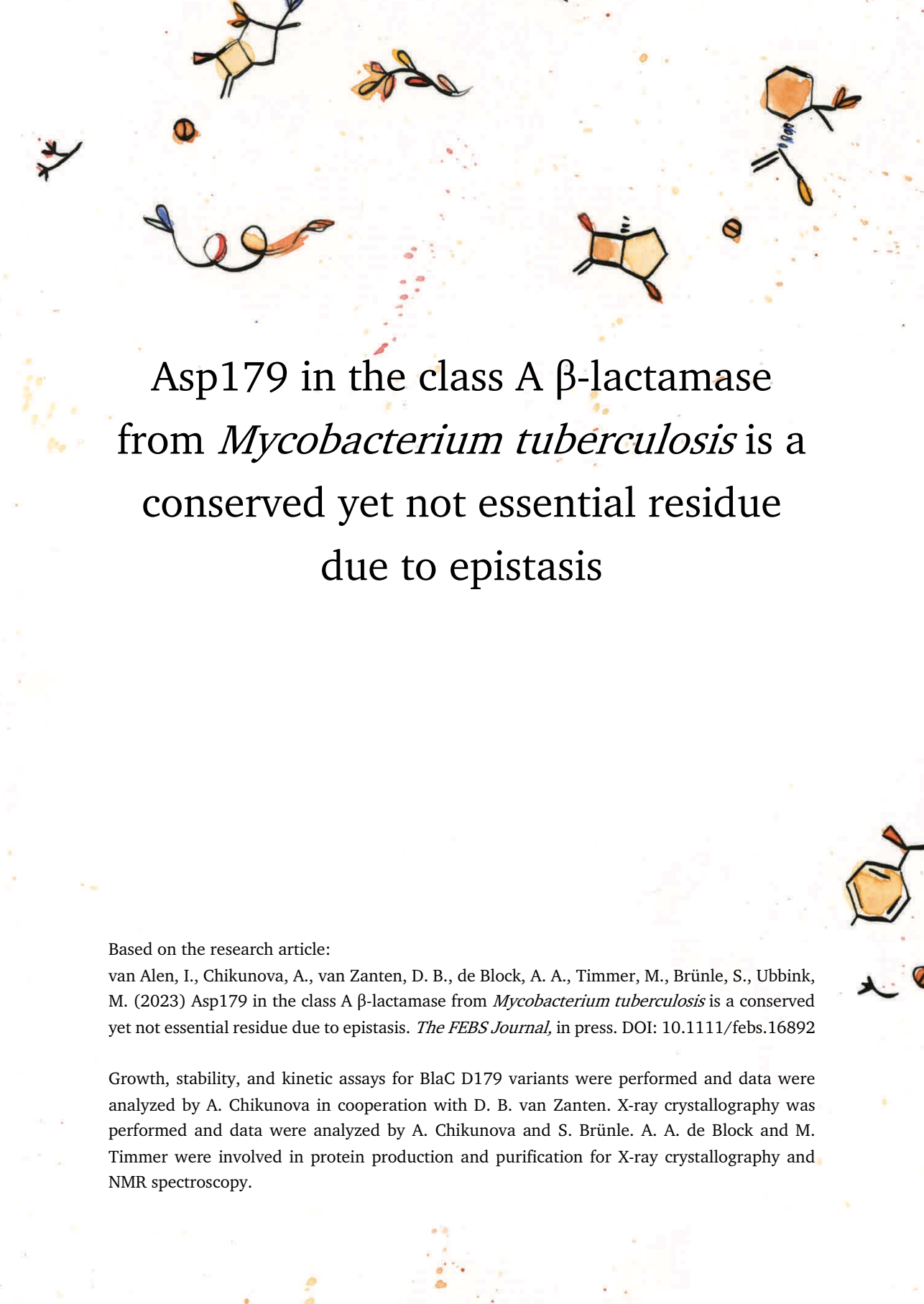
License: [Licence agreement concerning inclusion of doctoral thesis in the Institutional Repository of the University of Leiden](#)

Downloaded from: <https://hdl.handle.net/1887/3641470>

**Note:** To cite this publication please use the final published version (if applicable).

3





# Asp179 in the class A $\beta$ -lactamase from *Mycobacterium tuberculosis* is a conserved yet not essential residue due to epistasis

Based on the research article:

van Alen, I., Chikunova, A., van Zanten, D. B., de Block, A. A., Timmer, M., Brünle, S., Ubbink, M. (2023) Asp179 in the class A  $\beta$ -lactamase from *Mycobacterium tuberculosis* is a conserved yet not essential residue due to epistasis. *The FEBS Journal*, in press. DOI: 10.1111/febs.16892

Growth, stability, and kinetic assays for BlaC D179 variants were performed and data were analyzed by A. Chikunova in cooperation with D. B. van Zanten. X-ray crystallography was performed and data were analyzed by A. Chikunova and S. Brünle. A. A. de Block and M. Timmer were involved in protein production and purification for X-ray crystallography and NMR spectroscopy.

## Abstract

Conserved residues are often considered essential for function, and substitutions in such residues are expected to have a negative influence on the properties of a protein. However, mutations in a few highly conserved residues of the  $\beta$ -lactamase from *Mycobacterium tuberculosis*, BlaC, were shown to have no or only limited negative effect on the enzyme. One such mutant, D179N, even conveyed increased ceftazidime resistance upon bacterial cells, while displaying good activity against penicillins. The crystal structures of BlaC D179N in resting state and in complex with sulbactam reveal subtle structural changes in the  $\Omega$ -loop as compared to the structure of wild-type BlaC. Introducing this mutation in four other  $\beta$ -lactamases, CTX-M-14, KPC-2, NMC-A, and TEM-1, resulted in decreased antibiotic resistance for penicillins and meropenem. The results demonstrate that the Asp in position 179 is generally essential for class A  $\beta$ -lactamases but not for BlaC, which can be explained by the importance of the interaction with the side chain of Arg164 that is absent in BlaC. It is concluded that Asp179 though conserved is not essential in BlaC, as a consequence of epistasis



## Introduction

In protein families sets of highly conserved amino acid residues can be identified. Conservation is used as a proxy for essentiality because mutations in these residues are evidently not tolerated due to loss of function. The equation of conservation and essentiality is valid as an argument to explain conservation, but it does not mean that a conserved residue is essential in every member of the protein family. Epistatic effects influence the role of residues, and the essential nature of the residue may be lost without the residue being mutated. An example of such a case is described here. In a recent study from our laboratory, all the second and third-shell conserved residues in the class A  $\beta$ -lactamase BlaC from *Mycobacterium tuberculosis* were mutated.<sup>127</sup> In line with expectation, mutation of most conserved residues resulted in a non-functional enzyme. The distance from the active site was correlated with the function of the residues. Third-shell conserved residues, far from the active site, were shown to be essential for solubility and folding. Second-shell residues, around the active site, contribute to stabilizing the single catalytically most active conformation.<sup>127</sup> Interestingly, this broad mutagenesis study also revealed that for some conserved residues, certain mutations functioned equally or better than the wild-type enzyme in activity against ampicillin, raising the question of whether these conserved residues were essential.

Here, we focus on residue Asp179 (Ambler numbering<sup>65</sup>), which is present in 99.8% of the enzymes in this family.<sup>127</sup> Asp179 is located in the  $\Omega$ -loop of the protein, a loop that also contains Glu166, the general acid/base involved in deacylation of the enzyme, which is the second step in the catalytic mechanism.<sup>53,68,160</sup> In BlaC, the mutation D179N led to an increase in resistance against penicillins in *Escherichia coli* cells, together with a slightly increased thermostability of the enzyme.<sup>127</sup> However, the substitution of any other residue for Asp179 in TEM-1 and KPC-2 has been reported to result in less fitness, except when using ceftazidime as a substrate.<sup>161–166</sup> These results lead to the hypothesis that Asp179 is essential in other  $\beta$ -lactamases but not in BlaC, despite being conserved. To test this idea, BlaC D179N was characterized in more detail, and its fitness was compared with the same variant constructed in several other  $\beta$ -lactamases, representative of the class A  $\beta$ -lactamase family. Our results show that the mutation D179N indeed decreases the general fitness of other  $\beta$ -lactamases, contrary to BlaC. The crystal structure of BlaC D179N offers an explanation for the loss of the essentiality of Asp179.

## Results

### **BlaC D179 variants show different substrate specificity than wild type**

To investigate the importance of the side chain in position 179 of BlaC, the Asp was mutated to Ala, Glu, Gly, Leu, Asn, and Gln. *E. coli* cultures producing Asp179 variants were tested for resistance against various antibiotic compounds. The minimum concentrations at which the cells could not grow were determined by applying drops of cell culture of OD<sub>600</sub> 0.3 – 0.0003 on agar plates, containing the penicillins ampicillin, carbenicillin, or penicillin G, or the third-generation cephalosporin ceftazidime (Figures 3.1, S3.1, and S3.2). For the evaluation of  $\beta$ -lactamase inhibitor susceptibility, 100  $\mu\text{g mL}^{-1}$  carbenicillin was used in combination with the  $\beta$ -lactam inhibitor sulbactam and non- $\beta$ -lactam inhibitor avibactam. The results indicate that almost all tested Asp179 mutants outperformed the wild type against ceftazidime. D179G mutant was shown to be the most effective, with a more than six-fold increase in the minimum concentration that inhibited growth (Figure 3.1a, Table S3.1), which is quite remarkable given that ceftazidime is considered a very poor substrate for BlaC and many class A  $\beta$ -lactamases. However, only cells producing BlaC D179N displayed increased growth in the presence of other  $\beta$ -lactam antibiotics (Figures 3.1b, S3.1, and S3.2, Table S3.1) and they also showed somewhat higher resistance to avibactam, which probably can be attributed to an increased conversion of carbenicillin that was used in combination with inhibitors (Figure 3.1c). It is concluded that mutation of Asp179 in BlaC shifts the substrate specificity from penicillins to ceftazidime, except for BlaC D179N, which outperforms wild-type BlaC on both types of substrates.

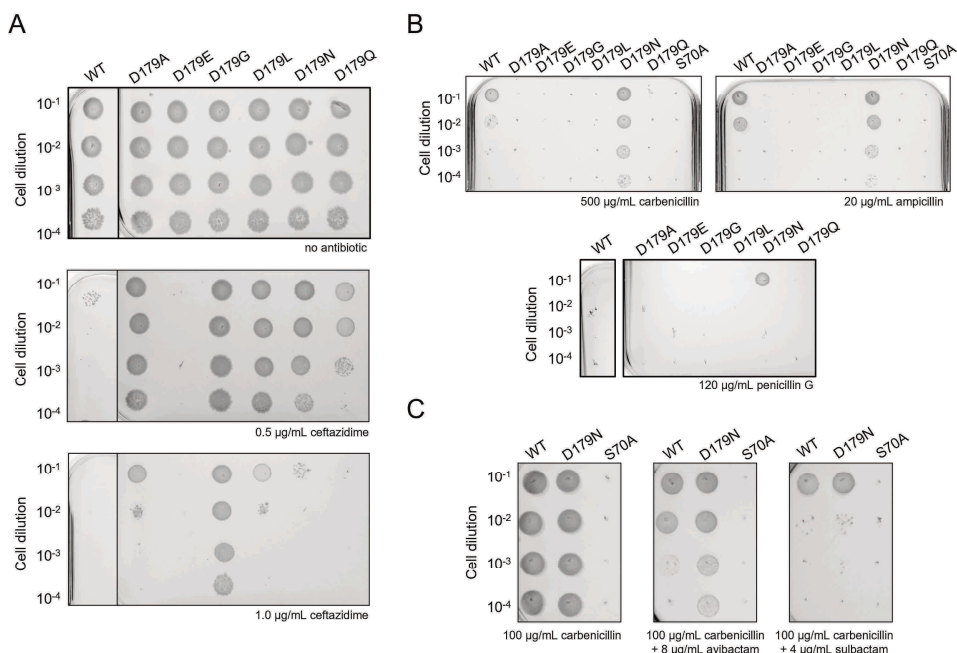


**Figure 3.1.** Cell growth assays. Drops of increasing dilutions of *E. coli* cultures were spotted on LB-agar plates containing the indicated antibiotics and inhibitors, as well as kanamycin ( $50 \mu\text{g mL}^{-1}$ ) to ensure plasmid stability and 1 mM IPTG to induce gene expression. The plates were incubated at  $37^\circ\text{C}$  for 16 h. (A) Ceftazidime. Wild-type BlaC panels are from the same LB-agar plates as BlaC variants (Figure S3.1 shows complete photos). (B) Carbenicillin, ampicillin, and penicillin G (Figures S3.1 and S3.2 show the complete data set). (C) Inhibitors subactam and avibactam in the presence of  $100 \mu\text{g mL}^{-1}$  carbenicillin. BlaC S70A is catalytically inactive and functions as a negative control.

### BlaC D179N has a higher melting temperature than wild type

To characterize the BlaC variants further, the enzymes were overproduced in *E. coli*. The yield of soluble BlaC D179E from one liter of cell culture was lower than for the other BlaC variants and most protein was insoluble (Figure 3.2a). Other BlaC variants were produced in quantities similar to the wild-type BlaC, except for BlaC D179N, for which production was slightly increased. All mutants, except for D179E, exhibited the same secondary structure content as wild-type BlaC, as judged by CD spectroscopy (Figure 3.2b). Denaturation experiments were performed to establish the thermal stability of the BlaC variants. Both tryptophan fluorescence and a thermal shift assay with hydrophobic dye were used for melting temperature assessment, as these methods might yield structure-specific results. Substitution of Asp179 with Asn resulted in a  $1.5^\circ\text{C}$  increase in melting temperature, whereas substitutions to Gly, Gln, and Ala significantly lowered melting temperature (Table 3.1, Figure 3.2b). Due to the poor sample quality, the melting temperature analysis was not possible for BlaC D179E and D179L. Slightly elevated levels of protein production together with a somewhat increased melting temperature of the D179N variant indicated improved overall stability of the protein.

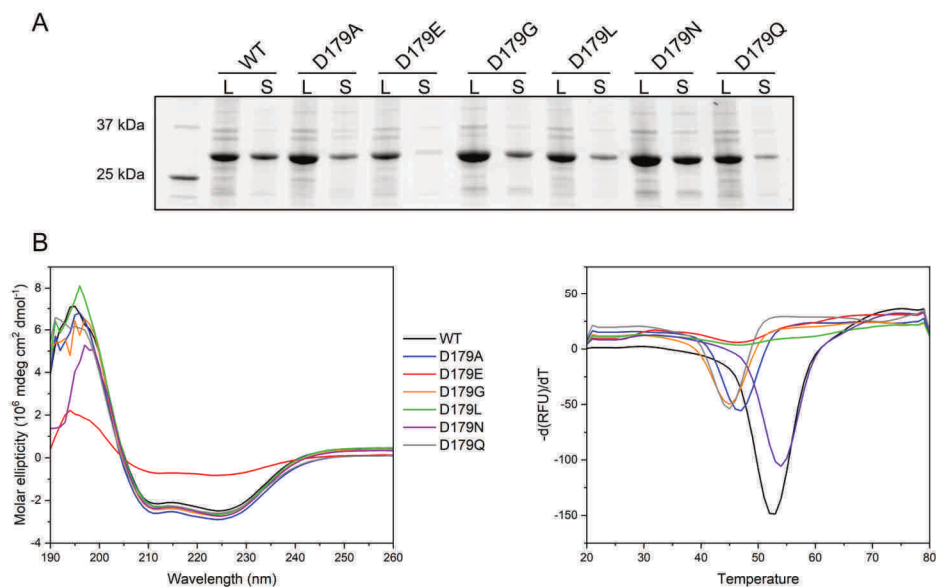


**Figure 3.2.** Production, folding, and stability of BlaC variants. (A) SDS-PAGE analysis shows the whole lysate (L) and soluble fraction (S) after the production of wild-type BlaC and BlaC D179 mutants. (B, left) CD spectra of BlaC Asp179 mutants. (B, right) Negative derivative of signal from thermal shift assay with the hydrophobic dye SYPRO® Orange of BlaC Asp179 mutants. The melting temperatures are listed in Table 3.1.

**Table 3.1.** Melting temperatures for BlaC variants. SD represents the standard deviation of three measurements. The two methods do not necessarily report the same conformational change making the melting temperature method-dependent.

BlaC variant	Tryptophan fluorescence		Hydrophobic dye	
	T <sub>m</sub> (SD) (°C)	Δ T <sub>m</sub> (SD) (°C)	T <sub>m</sub> <sup>a</sup> (°C)	Δ T <sub>m</sub> <sup>b</sup> (°C)
WT	62.0 (0.1)	0	52.0	0
D179A	54.8 (0.2)	-7.2 (0.2)	47.0	-5
D179G	51.4 (0.2)	-10.6 (0.2)	45.0	-7
D179N	63.3 (0.1)	1.3 (0.1)	53.5	1.5
D179Q	50.70 (0.05)	-11.3 (0.1)	45.0	-7

<sup>a</sup> Error 0.5 °C. <sup>b</sup> Propagated error 0.7 °C

### The increase in cell activity of BlaC D179N for most antibiotics is due to a more stable enzyme

The kinetic parameters of nitrocefin hydrolysis of BlaC D179N, BlaC D179G, and WT BlaC were measured using purified enzymes. BlaC D179N displayed nitrocefin activity very close to that of the wild-type BlaC with catalytic efficiencies of  $4.0 \pm 0.3 \times 10^5 \text{ M}^{-1} \text{ s}^{-1}$  and  $3.3 \pm 0.3 \times 10^5 \text{ M}^{-1} \text{ s}^{-1}$  for wild-type BlaC and BlaC D179N respectively (Table S3.2, Figure S3.3a). The *in vitro*

inhibition assay with avibactam indicated no increased resistance of this mutant against the inhibitor (Figure S3.3b). Therefore, we attribute the slight increase in activity against antibiotics in cells of BlaC D179N to an elevated production of a more stable enzyme, and the increased resistance of the cells to avibactam to the increased degradation of antibiotic. Purified BlaC D179G does not display any activity against nitrocefin (Figure S3.3c). However, ceftazidime activity benefits from both the Asp to Asn and Asp to Gly substitution (Table S3.2), with 2- and 80-fold increases of  $k_{cat}/K_M$  parameters, respectively. However, it is worth mentioning that ceftazidime remains a very poor substrate for all BlaC variants. Ceftazidime degradation with BlaC D179G displays two phases (Figure S3.3d), which makes it difficult to evaluate the reaction using a standard steady-state model. Here, we used the second linear phase to calculate the velocity of the reaction. Two-phase ceftazidime hydrolysis was explained before for KPC-2  $\beta$ -lactamase with the burst phase caused by rapid acylation and the following linear phase caused by slow diacylation.<sup>167</sup> This explanation does not apply to BlaC, as the amplitude of the burst phase indicates that the enzyme performs more than a single turnover and is substrate concentration dependent. It is probable that BlaC D179G exists in two conformations that react differently with ceftazidime. Such two-phase kinetics for ceftazidime has previously been published for TEM-1 W165Y/E166Y/P167G and PenI C69F and suggests a branched pathway for substrate hydrolysis.<sup>168,169</sup> This has also been observed for other BlaC variants (J. Sun and M. Ubbink, unpublished data) and will be described in more detail elsewhere.

### **BlaC D179N shows subtle conformational changes in comparison to wild type**

Structural characterization focused on BlaC D179N. NMR spectroscopy of BlaC D179N confirmed that this variant is well-folded (Figure S3.4). <sup>1</sup>H and <sup>15</sup>N chemical shifts of backbone amide resonances of the mutant protein were assigned and compared to those of wild-type BlaC (Figure 3.3). The largest chemical shift perturbations (CSPs) due to the mutation are observed for amides in the  $\Omega$ -loop but smaller CSPs spread out over other parts of the structure. The crystal structure of the BlaC D179N solved at 1.8 Å resolution reveals the nature of the structural changes (Table S3.3, Figures 3.4 and S3.5). Overall, the structure of the mutant resembles the structure of wild-type BlaC (C $\alpha$  RMSD 0.31 Å, Figure S3.5a). Surprisingly, the newly introduced asparagine occupies the same location as the side chain of aspartate (Figure S3.5b) and the interactions of D179 are conserved. In the structure of wild-type BlaC, the carboxy-carboxylate interaction requires a shared proton between Asp172 and Asp179,<sup>170,171</sup> in BlaC D179N this interaction likely is an ordinary hydrogen bond between the  $\gamma$ -carboxy group of Asp172 and NH<sub>2</sub> of the amide group of Asn179. Despite the conserved interactions, some changes are observed in the  $\Omega$ -loop of the mutant. Two peptide bonds, involving Pro174-Gly175 and Arg178-Asn179 are flipped in BlaC D179N (Figures 3.4a and 3.4b). The flipped bond involving Arg178 is accompanied by the loss of salt bridges between Arg178 and Asp172 and Asp163 and Arg161. Asp163 was found in two conformations, one of which is rotated towards the solvent, and the created space is occupied by the backbone carbonyl of Arg178. The second conformation is still able to form a salt bridge with Arg161, but both Asp163 and

Arg161 are pushed away from the loop containing Arg178. Previously, our group solved the structures of wild-type BlaC with the inhibitors clavulanic acid, sulbactam, tazobactam, and avibactam, as well as BlaC G132S with sulbactam.<sup>104,172</sup> Here, we solved the structures of BlaC D179N with inhibitors sulbactam and vaborbactam at 1.9 Å, as well as the structure of wild-type BlaC with vaborbactam (Figures S3.5c and S3.5d) as no structures of BlaC with this transition state inhibitor were available. Both inhibitors occupied the binding pocket of the BlaC D179N in the same way as in the wild-type enzyme (Figures S3.5e and S3.5f). In the structure of BlaC D179N with sulbactam, however, only the Pro174-Gly175 peptide bond was found flipped, while in the structure of BlaC D179N with vaborbactam both Pro174-Gly175 and Arg178-Asn179 were found in the same conformation as in the wild-type BlaC (Figure 3.4c). This indicates the increased conformational freedom of this region of the Ω-loop in BlaC D179N compared to the wild-type enzyme.

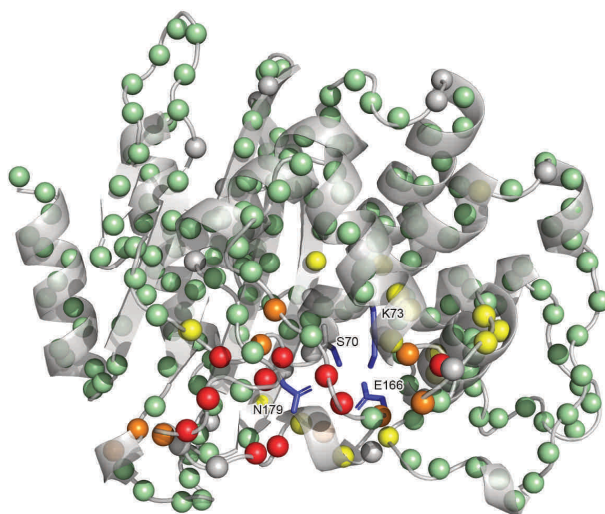


**Figure 3.3.** Average chemical shift differences (CSP) between the amide resonances of BlaC D179N and wild-type BlaC mapped on the structure of BlaC D179N (PDB entry 8BTU). Residues are colored green for CSP < 0.025, yellow for CSP > 0.025 ppm, orange for CSP > 0.05 ppm, red for CSP > 0.1 ppm, and gray for no data, backbone amide nitrogen atoms are represented as spheres. Side chains of active site residues and N179 are represented as blue sticks, the entrance to the active site is at the back of the protein in this representation.

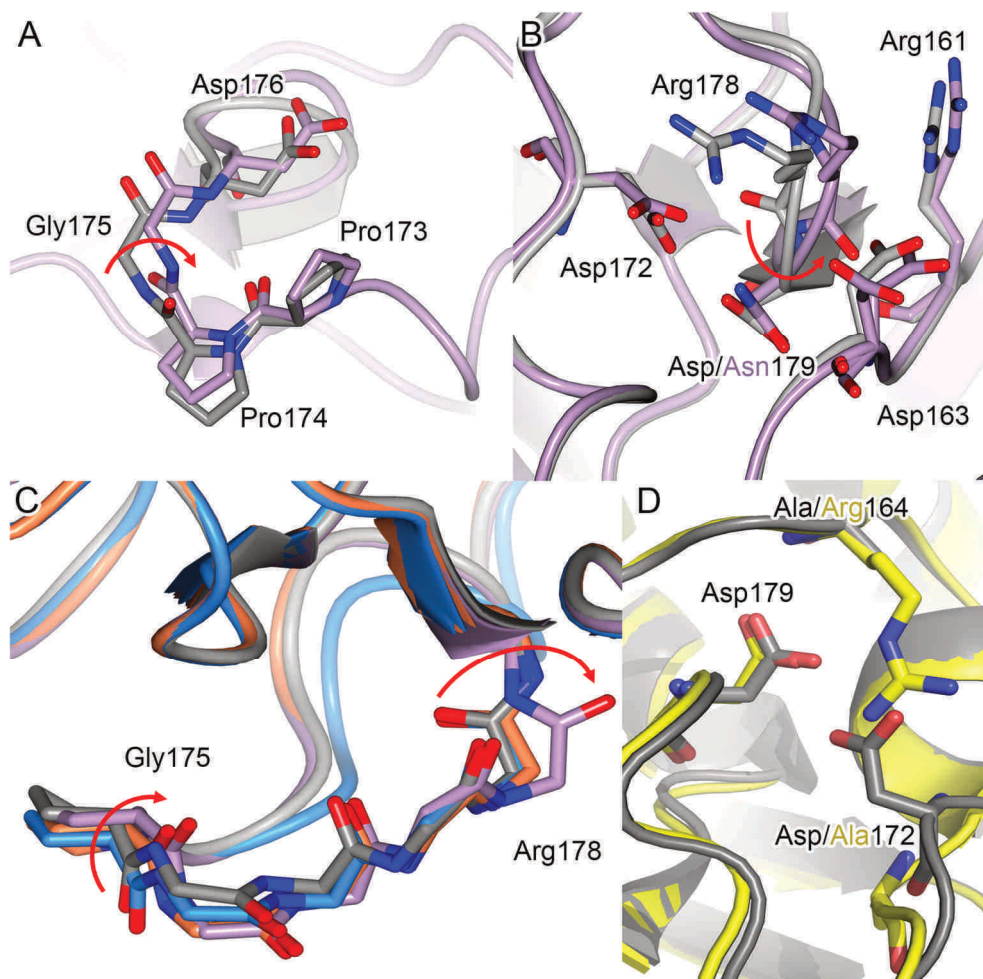


**Figure 3.4.** (A, B) Crystal structure of BlaC D179N (PDB entry 8BTU, lilac) overlaid with wild type structure (PDB entry 2GDN<sup>53</sup>, gray), showing the flipped peptide bonds between residues 174 and 175 (A) and 178 and 179 (B). The side chain of Asp163 in BlaC D179N is present in two conformations. (C) Crystal structure of wild-type BlaC (gray) overlaid with BlaC D179N free form (lilac), with sulbactam adduct (PDB entry 8BTU, orange) and vaborbactam (PDB entry 8BTW, blue). The backbone of the residues 174-179 is shown in sticks. The red arrows indicate the flipped peptide bonds. (D) Overlay of wild-type BlaC (gray) and TEM-1 (PDB entry 1ZG4<sup>126</sup>, yellow) showing the position of the residues 164, 172, and 179. In BlaC the side chain of Asp172 fills part of the space taken by the side chain of Arg164 in TEM-1.

### **The D179N mutation is detrimental in other class A $\beta$ -lactamases**

To investigate why residue 179 does not appear as an asparagine in class A  $\beta$ -lactamases, the D179N mutation was introduced in four BlaC orthologues. These  $\beta$ -lactamases were selected based on sequence identity (Table S3.4, Figure S3.6), structural root-mean-square deviation (RMSD), and available information from previous research. CTX-M-14, KPC-2, NMC-A, and TEM-1 share on average 42% of their sequences with BlaC, which is less than the average sequence identity of 50% found for 497 class A  $\beta$ -lactamase sequences. The average RMSD for the C $\alpha$  atoms of CTX-M-14, KPC-2, NMC-A, and TEM-1 compared to BlaC is 0.79 Å (Table S3.4). The genes coding for the soluble parts of these  $\beta$ -lactamases and their D179N variants were cloned in the same expression vector as *blaC*, behind a signal peptide for Tat-based translocation.<sup>172</sup> The ability to convey resistance to *E. coli* against antibiotics was tested as described for the BlaC variants. For both ampicillin and meropenem, the cells expressing the wild-type variants of CTX-M-14, KPC-2, NMC-A, and TEM-1 grow better than the cells expressing D179N variants, whereas this is not the case for BlaC (Figures 3.5, S3.7, and S3.8). This trend was also observed for carbenicillin, although NMC-A did not confer any resistance at the concentrations used for this assay (Figures 3.5 and S3.9). Interestingly, cells expressing the D179N variants for carbapenemases NMC-A and KPC-2 grow better on ceftazidime than cells expressing the wild-type variant, whereas cells expressing TEM-1 did not grow at all on the concentrations tested (Figures 3.5 and S3.10). These differences in growth were also observed when growing the cells in liquid cultures (Figures S3.11-S3.14). Cells producing TEM-1 grow worse in the presence of ampicillin than ones producing BlaC, which is surprising because TEM-1 is known to be quite active against ampicillin. Perhaps the expression system used in this study is less suitable for TEM-1 than for BlaC. So, in summary, the D179N mutation negatively affects the survivability of the cells producing all four  $\beta$ -lactamases, CTX-M-14, KPC-2, NMC-A, and TEM-1, in the presence of penicillins and meropenem, contrary to what was observed for BlaC.



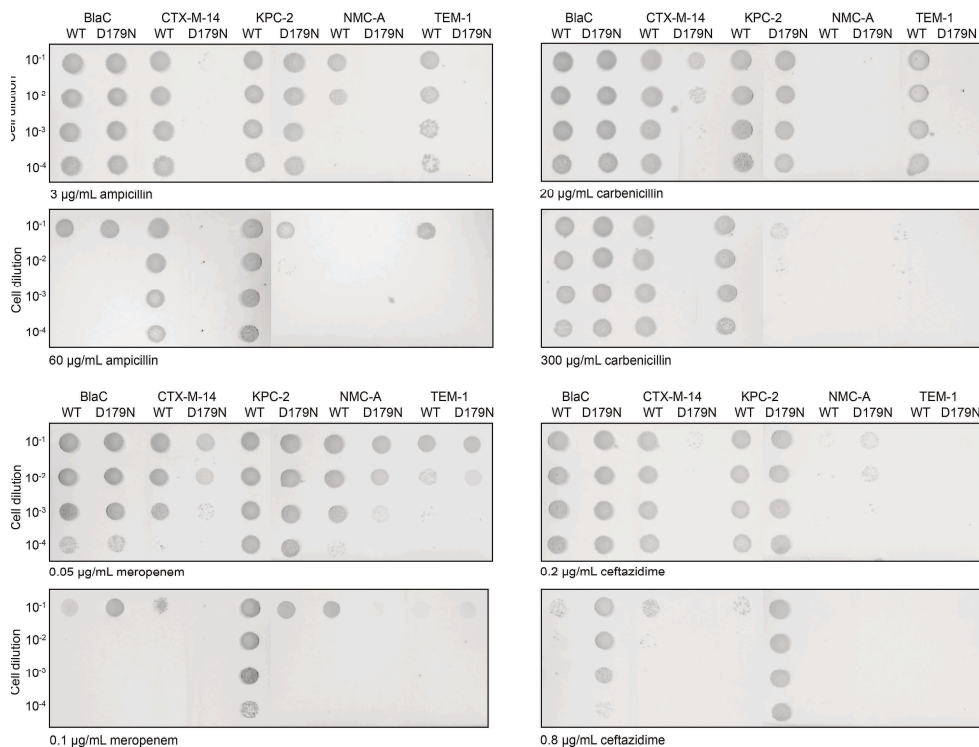


**Figure 3.5.** Activity against antibiotics of five class A  $\beta$ -lactamases. Cultures of *E. coli* expressing genes of the wild type or D179N variants of  $\beta$ -lactamases BlaC, CTX-M-14, KPC-2, NMC-A, or TEM-1 were spotted in increasing dilution on plates containing ampicillin, carbenicillin, meropenem or ceftazidime. Different panels within the black border originate from different parts of the same LB-agar plates (Figures S3.7-S3.10).

The *in vitro* activity of the  $\beta$ -lactamases was tested using the soluble cell fractions and nitrocefin as substrate, following an approach described before.<sup>127</sup> For these experiments, the genes were cloned in overexpression vectors with T7 promoter and cytoplasmic expression, as used for the BlaC production. Wild-type BlaC and BlaC D179N exhibit comparable protein levels and nitrocefin activity. However, large differences were observed for the other  $\beta$ -lactamases (Figure 3.6). Wild-type CTX-M-14 and TEM-1 were better at nitrocefin hydrolysis than BlaC while their D179N variants were insoluble, and no activity could be detected in the soluble cell fraction. Similarly, for KPC-2 and NMC-A the SDS-PAGE analysis shows the presence of more wild-type than mutant protein in the soluble cell fraction (Figure 3.6a), indicating that mutation D179N influences the stability of the enzyme.

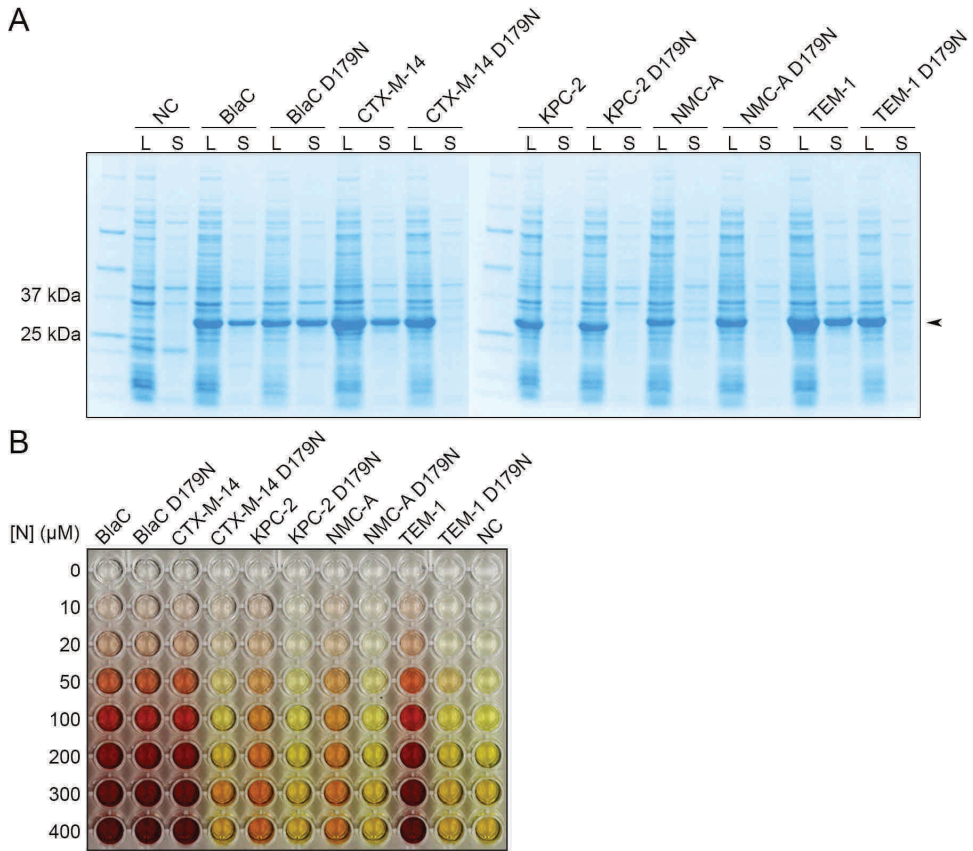


**Figure 3.6.** Effects of D179N mutation on several  $\beta$ -lactamases. (A) SDS-PAGE analysis shows the whole lysate (L) and soluble fractions (S) of negative control (NC), BlaC (31.5 kDa), CTX-M-14 (31.3 kDa), KPC-2 (31.8 kDa), NMC-A (32.4 kDa), and TEM-1 (32.2 kDa), indicated by an arrow. Samples were corrected for cell density. (B) Activity in nitrocefin conversion using soluble cell fractions of cultures overproducing the indicated  $\beta$ -lactamases was measured in 96-well plates containing the indicated nitrocefin (N) concentration. Upon ring opening, nitrocefin turns from yellow to red. The picture was taken 30 minutes after the start of the reactions.

## Discussion

The most common side chain interactions observed in the  $\Omega$ -loop of class A  $\beta$ -lactamases are Arg161-Asp163, Glu166-Asn170, and Arg164-Asp179. BlaC does not carry Arg at position 164, thus the latter salt bridge is missing. The importance of this salt bridge was discussed in multiple studies on various class A  $\beta$ -lactamases. It was shown that mutations in both Arg164 and Asp179 increase resistance against ceftazidime while decreasing the resistance to other  $\beta$ -lactam antibiotics.<sup>163,167,173–176</sup> The same effect is observed in our study on BlaC because almost all mutants of Asp179 cause increased resistance against ceftazidime in *E. coli* and decreased resistance to other compounds. Increased flexibility of  $\Omega$ -loop has been suggested as an explanation for the shift in substrate profile. A higher ceftazidime minimal inhibitory concentration was also reported for mutant P167S of CTX-M-14, and it was shown that this mutation causes conformational flexibility in the  $\Omega$ -loop and a large rearrangement of the loop in the acyl-enzyme complex.<sup>177</sup> In the resting state enzyme the loop was structurally similar to that in the wild-type protein, but with acylated adduct it assumed a different conformation, changing the position of the adduct compared to the adduct in the structure of the wild-type enzyme and so influencing the positions of active site residues. We observed similar behavior for the same mutation in BlaC, showing that indeed the conformational freedom introduced by this mutation is the reason for its changed substrate profile (J. Sun and M. Ubbink, unpublished data). The two-phased product formation curve and low melting temperature observed for BlaC D179G (Table 3.1, Figure S3.3d) resemble the behavior of BlaC P167S and suggest that also this variant exists in more than one conformation, either in the resting state or during the reaction (branched kinetics). Also, for other  $\beta$ -lactamases, studies indicate that mutation in D179 enhances the flexibility of the  $\Omega$ -loop. Barnes and colleagues<sup>166</sup> used modeling to predict the changes in the  $\Omega$ -loop occurring upon mutation of Asp179 in KPC-2, indicating loss of the interaction with Arg164 and increased flexibility of the  $\Omega$ -loop. This mobility led to changes in the position of the catalytic residues Ser70 and Glu166. The crystal structure of KPC-2 D179N showed that the disruption of 179-164 interaction results in a displacement of the active site residue Asn170.<sup>161</sup> This change was accompanied by a drastic decrease in the stability of the protein. The studies on the KPC D179Y variant showed that this mutation leads to a disordering of the  $\Omega$ -loop, which was linked to an improved ceftazidime degradation.<sup>161,178</sup> Increased flexibility of the  $\Omega$ -loop was also observed in the crystal structure of PC1 D179N from *Staphylococcus aureus*, where the  $\Omega$ -loop was found to be disordered.<sup>179</sup> In the case of BlaC Asp179 variants the increased conformational freedom of the part of the  $\Omega$ -loop can be explained by the change in the interaction between Asp172 and residue at position 179. Crystal structures of D179N BlaC indicated the possibility for the peptide bonds between these two residues to flip, which is likely caused by a new hydrogen bond Asn179-Asp172 interaction, which may be less rigid than the carboxyl-carboxylate bond in the wild type. Similarly, the absence of this bond in BlaC D179G might lead to even more conformational freedom in the  $\Omega$ -loop. Although NMR data did not support increased flexibility of the  $\Omega$ -loop in the D179N variant, the changes in the peptide bonds observed in the crystal structures can be an indication

of the ability of this variant to adapt the conformation of the loop to the specific substrate or inhibitor, which can also explain changed substrate specificity of the Asp179 variants towards the bulky substrate ceftazidime.

Here, we tested the effects of D179N in five  $\beta$ -lactamases that are representative of the class A  $\beta$ -lactamases. The mutants of KPC-2, NMC-A, and TEM-1 show decreased survivability of *E. coli* producing these variants compared to wild type in the presence of both penicillins and meropenem and improved survivability in the presence of ceftazidime, in line with fitness studies on TEM-1 and KPC-2.<sup>163,166</sup> In CTX-M-14, the D179N substitution impacts the ability of the cells producing this variant to grow in presence of all tested antibiotics, probably because the solubility of the enzyme is compromised by the mutation. These findings, together with the previous findings described in literature, suggest that in all cases the  $\Omega$ -loop is more mobile, enhancing activity against ceftazidime or, in the case of CTX-M-14, to such an extent that the protein is no longer stable and becomes insoluble. These observations make BlaC D179N an interesting exception. Mutation to other residues of Asp179 in BlaC also leads to a reduced melting temperature and a shift in the substrate spectrum toward ceftazidime activity. BlaC D179N, however, is produced as a soluble protein with high yield, shows a single conformation in the NMR spectrum, with no evidence of extensive line-broadening, and yields a crystal structure with an ordered  $\Omega$ -loop. At the same time, it shows somewhat enhanced activity against ceftazidime as well as good activity against penicillins and nitrocefin. Position 164 is occupied predominantly by Arg in class A  $\beta$ -lactamases, while BlaC carries Ala at this position. The H-bond between Asp172 and Asp179 in BlaC is only possible due to the absence of Arg at position 164 because the side chains of Arg164 and Asp172 would clash (Figure 3.4d). This subtle change could be responsible for differences observed upon mutation in Asp179 in BlaC vs. other  $\beta$ -lactamases. The D179N in BlaC appears to strike a balance that enhances stability and yet slightly increases  $\Omega$ -loop flexibility. In other  $\beta$ -lactamases, the mutation introduces flexibility and reduced stability due to the lost salt bridge between Asp179 and Arg164. Asp179 is highly conserved in class A  $\beta$ -lactamases, and so is Arg164, thus it is possible that being able to cope with the loss of this Arg, opens a new evolutionary pathway to BlaC by introducing the D179N mutation to stabilize the enzyme and at the same time enhance its substrate spectrum.

## Materials and methods

### $\beta$ -Lactamase activity in bacterial cells

Resistance assays were performed with *E. coli* KA797 cells transformed with pUK21-based plasmids with a Tat-signal sequence<sup>172</sup> and containing the *blaC*, *blaCTX-M-14*, *kpc*, *nmcA* or *bla* wild-type or mutant genes, coding for the soluble parts of BlaC, CTX-M-14, KPC-2, NMC-A, and TEM-1, respectively (Figure S3.6). For the on-plate assay, cells were applied on the agar plates with various  $\beta$ -lactam antibiotics as 10  $\mu$ L drops with OD<sub>600</sub> values of 0.3, 0.03, 0.003, and 0.0003. All plates contained 50  $\mu$ g mL<sup>-1</sup> kanamycin and 1 mM IPTG and were incubated for 16 h at 37 °C. The IPTG was used in the plates for continuity, as previous experiments in the group were conducted in the presence of IPTG. However, the addition of IPTG did not result in overexpression of the protein, and the expression of  $\beta$ -lactamases remained constant and constitutional throughout the experiment. For the assay with bacterial suspensions, cells with the OD<sub>600</sub> 0.3 were diluted 100-fold in LB medium and incubated overnight at 37 °C with constant shaking. Measurements were performed with a Bioscreen C plate reader.

### Protein production and purification

$\beta$ -Lactamases were produced using *E. coli* BL21 (DE3) pLysS cells transformed with pET28a plasmids containing the T7 promotor, the same genes as used for the bacterial cell assays (Figure S3.6), with an N-terminal His-tag and TEV cleavage site.<sup>172</sup> BlaC was produced and purified as described previously.<sup>81</sup> For experiments comparing wild-type and D179N variants of various  $\beta$ -lactamases, the pellets from 10 mL overnight cultures were lysed in 200  $\mu$ L of BPER (Thermo Scientific, Rockford, USA) for 30 min. After centrifugation, the soluble fraction was diluted 50-fold in 100 mM sodium phosphate buffer (pH 6.4) and used for circular dichroism spectroscopy and kinetic experiments. Protein solubility was determined by running samples of the whole lysate and the soluble fraction on a 4–15% Mini-PROTEAN TGX Stain-Free Protein Gel (BioRad, Hercules, USA). The proteins were overproduced in the soluble form without the signal peptide for better visualization on the gel.

### Circular dichroism spectroscopy

Circular dichroism spectra were recorded in a 1 mm quartz cuvette at 25 °C with a Jasco J-815 spectropolarimeter. Samples contained 100 mM sodium phosphate buffer (pH 6.4). The curves represent the average of five transients.

### Melting temperature

The thermostability of BlaC variants was determined with the use of the hydrophobic dye SYPRO® Orange (Sigma-Aldrich, St. Louis, USA) or using tryptophan fluorescence changes. The commercially available stock of SYPRO® Orange dye has a 5000x concentration, but a 4x concentration was used in the measurements. Tryptophan fluorescence was measured as a function of temperature using a Tycho NT.6 (NanoTemper Technologies, München, Germany)

at 330 nm and 350 nm and the ratio 330 nm/350 nm was used to evaluate the melting temperature. All measurements were done in triplicate in 100 mM sodium phosphate buffer (pH 6.4).

## Kinetics

Kinetic experiments for BlaC D179 variants were performed using a Lambda 800 UV-vis spectrometer (PerkinElmer, Waltham, USA) at 25 °C in 100 mM sodium phosphate buffer (pH 6.4). For nitrocefin kinetics 5 nM of enzyme was used with 0 μM, 10 μM, 25 μM, 50 μM, 100 μM, 200 μM, 300 μM, and 400 μM of nitrocefin ( $\Delta\epsilon_{486} = 18 \times 10^3 \text{ cm}^{-1} \text{ M}^{-1}$ ). The reactions were followed at 486 nm for 90 seconds in triplicate. The initial velocities were fitted to the Michaelis-Menten, equation 3.1.  $v_0$  is the initial reaction rate,  $[S]_0$  the initial substrate concentration,  $V_{\max}$  the maximum reaction rate, and  $K_M$  the Michaelis-Menten constant.  $v_0$  and  $[S]_0$  are the dependent and independent variables, respectively, and  $K_M$  and  $V_{\max}$  are the fitted parameters.  $V_{\max}$  is equal to the product of the specific rate constant ( $k_{\text{cat}}$ ) and the enzyme concentration.

$$v_0 = \frac{V_{\max} [S]_0}{K_M + [S]_0} \quad (3.1)$$

To measure the hydrolysis of ceftazidime for Figure S3.3d, 1 μM of BlaC was mixed with 20 μM ceftazidime. Substrate degradation was followed at 260 nm for 7 minutes in duplicate. The extinction coefficient difference ( $\Delta\epsilon_{260}$ ) was determined to be  $6.8 \pm 0.9 (\times 10^3) \text{ M}^{-1} \text{ cm}^{-1}$  (J. Sun, personal communication). The kinetic parameters of the ceftazidime hydrolysis reaction were determined with 100 nM of BlaC and 10 μM, 25 μM, 50 μM and 100 μM of ceftazidime. The reactions were followed at 260 nm for 5 minutes and performed in duplicate. Due to the biphasic behavior of the reaction the velocities of the second phase were calculated and plotted against substrate concentration. For wild-type BlaC and BlaC D179N, the determination of the  $K_M$  and  $V_{\max}$  values was not possible because  $K_M \gg [S]$ , so  $k_{\text{cat}}/K_M$  were determined from  $v_0/[S]$ . Activity in lysates was determined by mixing the 50x diluted soluble fraction of cell lysates with 0 μM, 10 μM, 20 μM, 50 μM, 100 μM, 200 μM, 300 μM and 400 μM of nitrocefin at 25 °C.

## Inhibition assay

To measure the BlaC inhibition by avibactam, 2.5 nM of BlaC was used with 100 μM nitrocefin in the presence of increasing amounts of avibactam, 0 μM, 10 μM, 100 μM, and 500 μM. The reactions were followed at 486 nm for 20 min and the experiments were performed in duplicate.

## NMR spectroscopy experiments

$^{13}\text{C}$ ,  $^{15}\text{N}$  enriched (98%) protein was produced as described previously.<sup>81</sup> TROSY-HSQC<sup>150,151</sup> and HNCA spectra were recorded on an AVIII HD 850 MHz spectrometer (Bruker Biospin, Leiden, The Netherlands) at 25 °C on a sample of 1 mM BlaC in 100 mM phosphate buffer (pH 6.4) with 6% D<sub>2</sub>O in a 5 mm NMR tube. Data were processed in Topspin 4.0.7 (Bruker Biospin). Spectra were analyzed with CCPNmr Analysis software V3.<sup>152</sup> Amide resonances were assigned for BlaC D179N by comparison to peaks in the wild-type BlaC spectrum<sup>81,148</sup> and confirmed using the HNCA spectrum. Average chemical shift perturbations (CSP),  $\Delta\delta$ , of the  $^1\text{H}$  ( $\Delta\omega_1$ ) and  $^{15}\text{N}$  ( $\Delta\omega_2$ ) resonances of backbone amides were calculated using equation 3.2:

$$\Delta\delta = \sqrt{\frac{1}{2}\left(\Delta\omega_1^2 + \left(\frac{\Delta\omega_2}{5}\right)^2\right)} \quad (3.2)$$

## Crystallization

Crystallization conditions for BlaC D179N at a concentration of 10 mg mL<sup>-1</sup> were screened for by the sitting-drop method using the JCSG+, BCS and Morpheus (Molecular Dimensions, Catcliffe, UK) screens at 20°C with 200 nL drops with 1:1 protein to screening condition ratio.<sup>153</sup> Crystal growth became visible within four days in various conditions specified in Table S1. After one month the crystals were mounted on cryoloops in mother liquor and vitrified by plunging in liquid nitrogen. The crystals of BlaC bound to the inhibitors were soaked in corresponding mother liquor with 10 mM sulbactam or vaborbactam for 20-40 minutes.

## X-ray data collection, processing, and structure solving

Diffraction data were collected at the Diamond Light Source (DLS, Oxford, England). Diffraction data were recorded on a Pilatus detector. The resolution cutoff was determined based on completeness and CC1/2 values. The data were integrated using DIALS<sup>180</sup> and scaled using Aimless.<sup>155</sup> The structures were solved by molecular replacement using MOLREP from the CCP4 suite<sup>156</sup> using PDB entry 2GDN<sup>53</sup> as a search model for all structures except for BlaC D179N with sulbactam for which 6H2K<sup>104</sup> was used as a search model. Subsequently, building and refinement were performed using Coot and REFMAC.<sup>156</sup> Waters were added in REFMAC during refinement. The following residues were modeled in two conformations: Asp163 for BlaC D179N, Lys230 for BlaC D179N with sulbactam, and Asn197 for BlaC D179N with vaborbactam. The final models fall on the 98<sup>th</sup>-99<sup>th</sup> percentile of MolProbity.<sup>158</sup> The models were further optimized using the PDB-REDO webserver.<sup>157,159</sup> Structure validation showed a RamaZ score<sup>159</sup> of -0.15, -0.27, -0.44, and -1.82 for D179N, D179N with sulbactam, D179N with vaborbactam, and wild-type BlaC with vaborbactam respectively; 97-99% of all residues are within the Ramachandran plot favored regions with two outliers for all structures, namely, Cys69 and Arg220. Data collection and refinement statistics can be found in Table S3.3.

## **Structural and sequential analysis**

Sequence identity was calculated by Clustal Omega<sup>181</sup> using 497 sequences of class A  $\beta$ -lactamases without signal sequence. 494 originate from the broad mutagenesis study,<sup>127</sup> which includes BlaC and CTX-M-14. The sequences of BlaC, CTX-M-14, KPC-2, NMC-A and TEM-1 correspond to Uniprot entries P9WKD3, Q9L5C7, Q9F663, P52663 and P62593, respectively. Structural analysis was done using the PDB structures 2GDN<sup>53</sup>, 1YLT<sup>182</sup>, 2OV5 (subunit A)<sup>183</sup>, 1BUE<sup>184</sup>, and 1ZG4<sup>126</sup> for BlaC, CTX-M-14, KPC-2, NMC-A, and TEM-1, respectively. Root mean square deviations (RMSD) were calculated by a sequence-independent structure-based alignment in The PyMOL Molecular Graphics System, Version 2.5.0 (Schrödinger, LLC, New York, USA).

## **Data availability**

NMR chemical shift assignments have been submitted to the Biological Magnetic Resonance Data Bank (BMRB) and can be accessed under BMRB accession number 51702. The crystal structures and data files of free-form BlaC D179N and BlaC D179N bound to sulbactam or vaborbactam and wild-type BlaC bound to vaborbactam have been submitted to the Protein Data Bank (PDB) and can be accessed under accession numbers 8BTU, 8BTV, 8BTW, and 8BV4, respectively.



## Supporting information

**Table S3.1.** Concentrations of various  $\beta$ -lactams and  $\beta$ -lactamase inhibitors at which growth of *E. coli* producing BlaC variants is no longer observed, determined with the droplet test (Figures 3.1, S3.1, and S3.2). All values are in  $\mu\text{g mL}^{-1}$ . Catalytically inactive BlaC S70A was used as a negative control.

BlaC variant	Ampicillin	Ceftazidime	Carbenicillin	Penicillin G	Avibactam <sup>a</sup>	Sulbactam <sup>a</sup>
WT	120	0.8	>1000	120	>16	5
S70A	3	0.2	20	40	NA	NA
D179A	10	2	100	80	NA	NA
D179E	3	0.2	20	40	NA	NA
D179G	5	5	100	40	NA	NA
D179L	3	2	20	40	NA	NA
D179N	120	2	>1000	>120	>16	7.5
D179Q	5	1	20	40	NA	NA

<sup>a</sup> Inhibitors were used in combination with  $100 \mu\text{g mL}^{-1}$  carbenicillin. NA, not applicable.

**Table S3.2.** Michaelis-Menten kinetic parameters for nitrocefin and ceftazidime hydrolysis. Reactions were carried out in 100 mM sodium phosphate buffer (pH 6.4) at 25 °C. Standard deviations (SD) are calculated from triplicate measurements for nitrocefin and duplicate measurements for ceftazidime. ND: Not determined.

BlaC variant	Nitrocefin			Ceftazidime		
	$K_M \pm \text{SD}$ ( $\mu\text{M}$ )	$k_{\text{cat}} \pm \text{SD}$ ( $\text{s}^{-1}$ )	$k_{\text{cat}}/K_M \pm \text{SD}$ ( $10^5 \text{ M}^{-1}\text{s}^{-1}$ )	$K_M \pm \text{SD}$ ( $\mu\text{M}$ )	$k_{\text{cat}} \pm \text{SD}$ ( $\text{min}^{-1}$ )	$k_{\text{cat}}/K_M \pm \text{SD}$ ( $10^3 \text{ M}^{-1}\text{s}^{-1}$ )
WT	$263 \pm 17$	$106 \pm 5$	$4.0 \pm 0.3$	ND	ND	$0.09 \pm 0.01$
D179N	$297 \pm 24$	$98 \pm 6$	$3.3 \pm 0.3$	ND	ND	$0.24 \pm 0.02$
D179G	ND	ND	ND	$1.1 \pm 0.1$	$0.6 \pm 0.1$	$7 \pm 2$

**Table S3.3.** Data collection and refinement statistics for BlaC D179N structures and BlaC WT with vaborbactam.

Data Collection	D179N	D179N + sulbactam	D179N + vaborbactam	WT + vaborbactam
PDB ID	8BTU	8BTV	8BTW	8BV4
Conditions	0.1 M ammonium acetate; 0.1 M BIS-TRIS buffer (pH 5.5); 17% w/v PEG 10K	0.1 M sodium phosphate/citrate (pH 5.5); 20% v/v PEGSH	0.1 M sodium phosphate buffer (pH 6.2); 0.2 M sodium formate; 20% v/v PEGSM	0.1 M bicine/Trizma buffer (pH 8.5); 0.09 M NPS; 30% w/v EDO-P8K
Wavelength (Å)	0.9795	0.9795	0.9795	0.9795
Resolution (Å)	38.31-1.80 (1.84-1.80)	53.81-1.95 (2.00-1.95)	44.93-1.90 (1.94-1.90)	44.78-1.95 (2.00-1.95)
Space group	P 1 21 1	P 1 21 1	P 21 21 21	P 21 21 21
Unit cell a, b, c (Å)	38.37, 54.05, 53.64	38.95, 54.73, 53.88	53.82, 54.45, 79.53	38.37, 54.05, 53.64
$\alpha, \beta, \gamma$	90.0, 93.2, 90.0	90.0, 92.9, 90.0	90.0, 90.0, 90.0	90.0, 93.2, 90.0
CC <sub>1/2</sub>	98.8 (59.1)	98.9 (68.2)	98.8 (60.3)	98.5 (70.3)
R <sub>pim</sub> (%)	9.1 (42.7)	8.5 (36.6)	9.7 (45.1)	12.4 (56.6)
I/ $\sigma$ I	5.2 (1.2)	5.7 (1.9)	5.3 (1.3)	6.5 (1.3)
Completeness (%)	98.4 (97.7)	100.0 (100.0)	99.9 (98.7)	99.9 (99.6)
Multiplicity	1.8	1.9	1.9	1.9
Unique reflections	20045	16630	19007	17259
Refinement				
Atoms protein/water	2000/0/207	2001/49/154	2000/54/185	1996/80/140
B-factors protein/water (Å <sup>2</sup> )	20/-/27	19/32/26	20/30/30	30/51/40
R <sub>work</sub> /R <sub>free</sub> (%)	18.0/23.8	17.1/20.5	16.1/20.2	20.0/23.2
Bond lengths RMSZ/RMSD (Å)	0.829/0.0084	0.436/0.0121	0.5/0.0095	0.65/0.01
Bond angles RMSZ/RMSD (°)	0.933/1.42	0.759/1.71	0.798/1.54	0.888/1.61
Ramachandran plot preferred/outliers	246/2	245/2	245/2	246/2
Ramachandran plot Z-score	-0.15	-0.27	-0.44	-1.82
Clash score	3.78	4.45	3.44	6.11
MolProbity score	1.17	1.22	1.14	1.34

**Table S3.4.** Sequence identity as determined by ClustalOmega and RMSD as determined by PyMOL when aligning by structure (Uniprot entries P9WKD3-1, Q9L5C7, Q9F663, P52663, P62593, and PDB entries 2GDN<sup>53</sup>, 1YLT<sup>182</sup>, 2OV5<sup>183</sup>, 1BUE<sup>184</sup>, and 1ZG4<sup>126</sup>).

		Sequence identity (%)					
		BlaC	CTX-M-14	KPC-2	NMC-A	TEM-1	<i>Average</i>
Structural RMSD (Å)	BlaC		45	48	41	35	42
	CTX-M-14	0.728		54	49	38	46
	KPC-2	0.771	0.569		58	40	50
	NMC-A	0.964	0.861	0.600		35	45
	TEM-1	0.702	0.638	0.693	0.927		37
	<i>Average</i>	0.791	0.699	0.658	0.838	0.740	

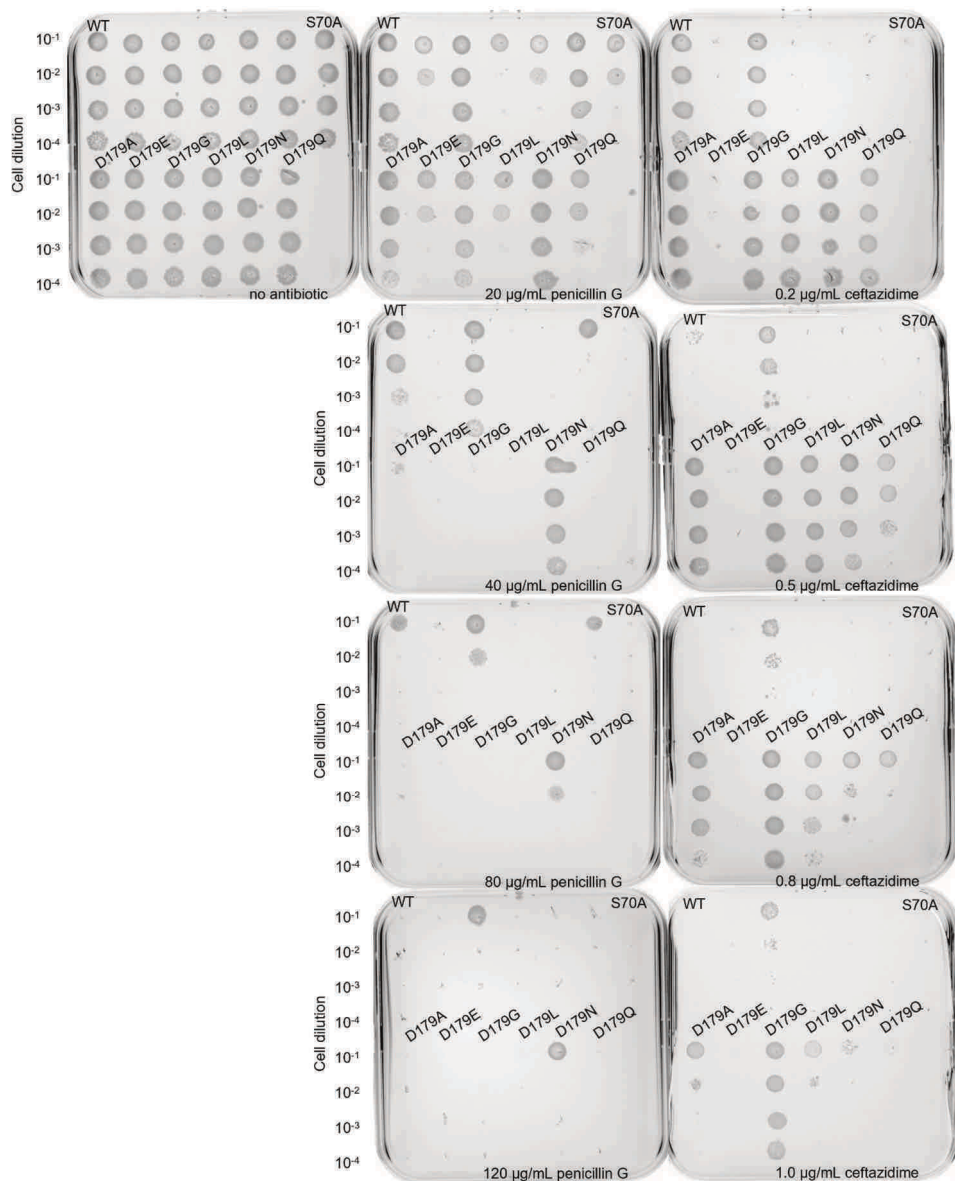


**Figure S3.1.** Activity against penicillin G and ceftazidime of BlaC Asp179 variants, wild-type BlaC, and inactive S70A BlaC as the negative control. Cultures of *E. coli* expressing genes of the BlaC variants were spotted in increasing dilution on plates containing various concentrations of penicillin G or ceftazidime. Non-labeled drops contain mutants of the residues not discussed within the scope of this thesis.

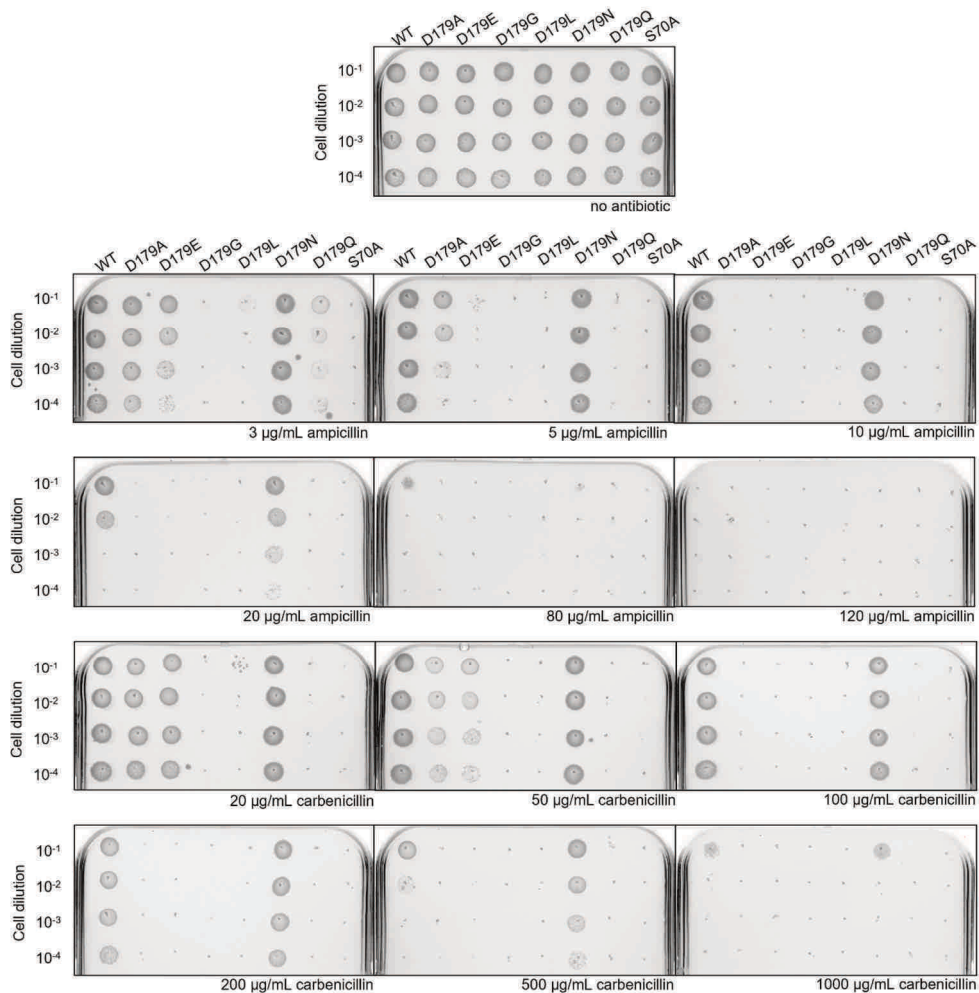


**Figure S3.2.** Activity against ampicillin and carbenicillin of BlaC Asp179 variants, wild-type BlaC and inactive S70A BlaC as the negative control. Cultures of *E. coli* expressing genes of the BlaC variants were spotted in increasing dilution on plates containing various concentration of ampicillin or carbenicillin.

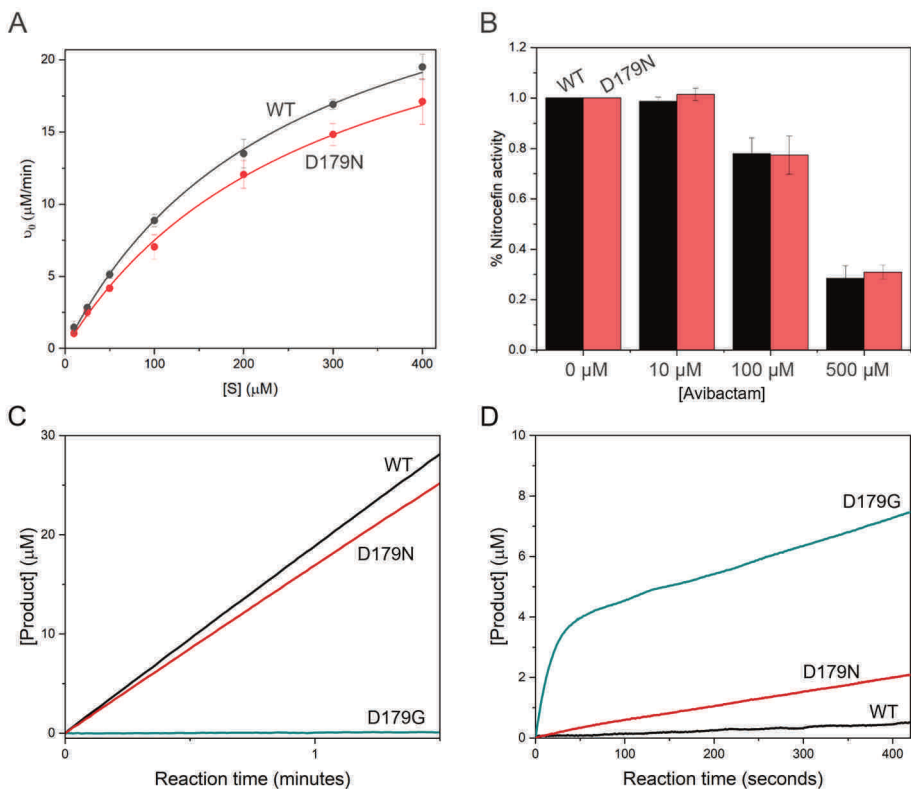


**Figure S3.3.** Kinetic analysis. (A) Michaelis-Menten curves for reaction with nitrocefin of wild-type BlaC and BlaC D179N. Error bars represent standard deviations of triplicates and curves represent the fit to the Michaelis-Menten equation (eq. 3.1). (B) Relative activity in the absence or presence of avibactam and BlaC is measured as the amount of hydrolyzed nitrocefin after 20 min at 25 °C. Measurements were performed in duplicate in the presence of 100  $\mu\text{M}$  nitrocefin and 2.5 nM BlaC. The error bars represent one standard deviation. (C) Product formation curves with 400  $\mu\text{M}$  nitrocefin and 5 nM BlaC as a function of time. (D) Product formation curves with 20  $\mu\text{M}$  ceftazidime and 1  $\mu\text{M}$  BlaC. Data were obtained in 100 mM sodium phosphate buffer (pH 6.4) at 25 °C by measuring a change in absorbance at 486 nm and 260 nm for nitrocefin and ceftazidime, respectively.

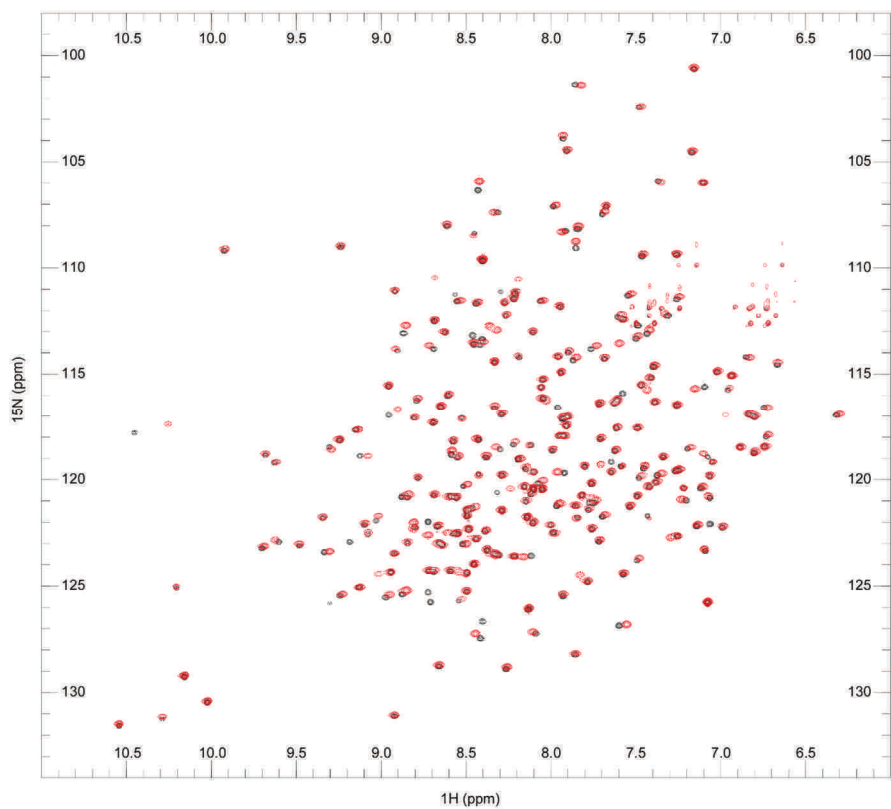


**Figure S3.4.** Overlay of  $^1\text{H}$ - $^{15}\text{N}$  TROSY-HSQC spectra for wild-type BlaC (black) and BlaC D179N (red).

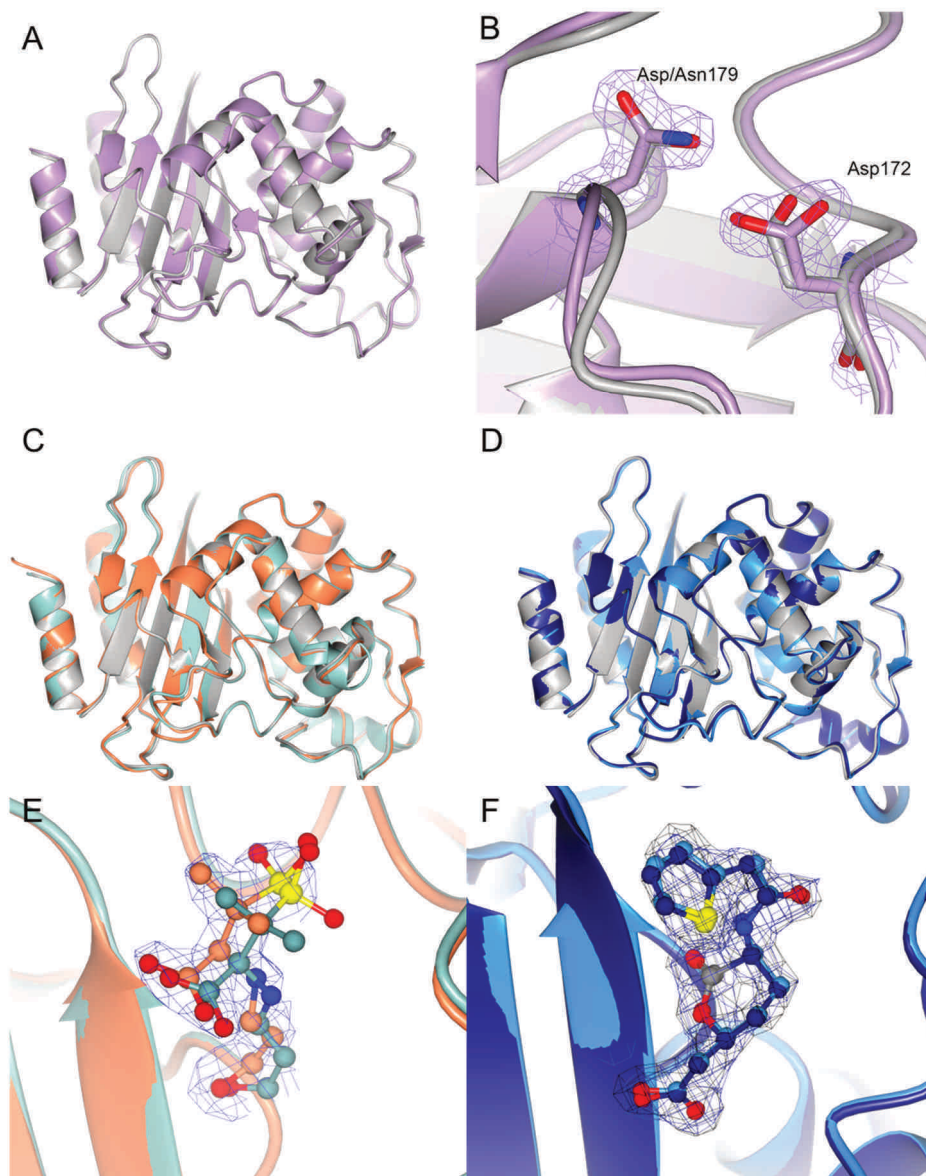


**Figure S3.5.** (A) Crystal structure of BlaC D179N (PDB entry 8BTU, lilac) overlaid with wild type structure (PDB entry 2GDN<sup>53</sup>, gray). (B) Detail of the region around the mutation. The 2mF0-DFc electron density map for BlaC D179N is centered on labeled residues and is shown in purple chicken wire, with contour level 1  $\sigma$  and extent radius 5 Å. (C) Crystal structure of BlaC D179N with sulbactam (PDB entry 8BTU, orange) overlaid with wild type structure free form (gray) and with sulbactam (PDB entry 6H2K<sup>104</sup>, light green). (D) Crystal structure of BlaC D179N with vaborbactam (PDB entry 8BTW, light blue) overlaid with wild type structure, free form (gray) and with vaborbactam (PDB entry 8BV4, dark blue). (E, F) position of inhibitors sulbactam (E) and vaborbactam (F), respectively in BlaC wild type (light green and dark blue, respectively) and BlaC D179N (orange and light blue, respectively). The 2mF0-DFc electron density maps with contour level 1  $\sigma$  and extent radius 5 Å are centered on inhibitor structures and are shown in blue chicken wire for BlaC D179N structures or black chicken wire for BlaC wild type with vaborbactam.



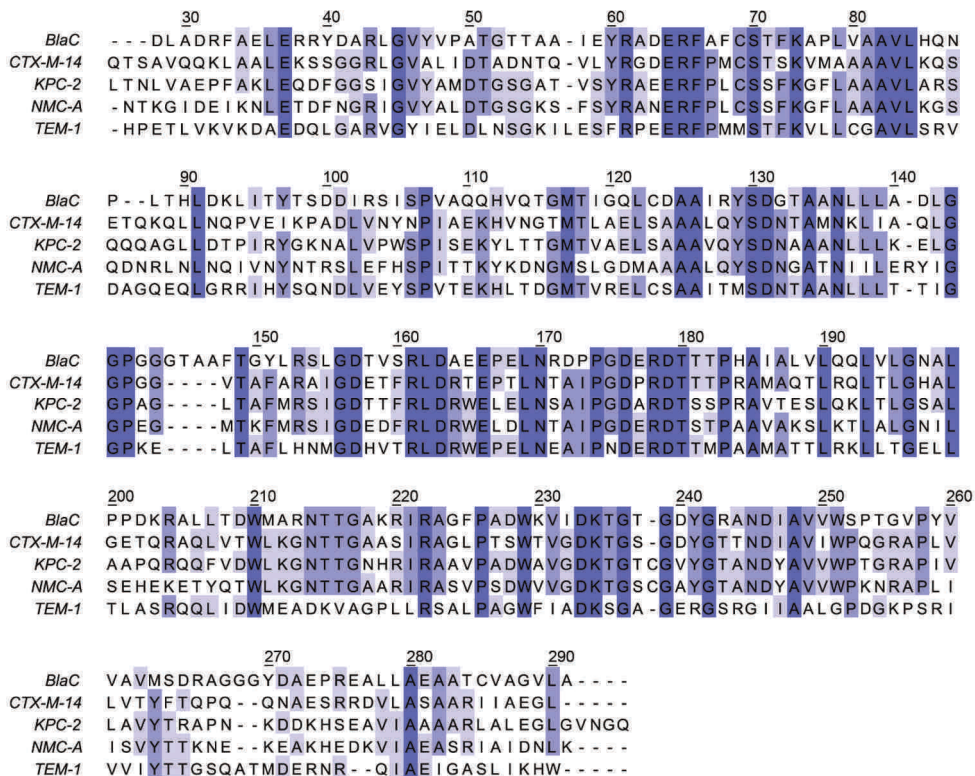


**Figure S3.6.** Sequences of  $\beta$ -lactamases. Residues are numbered according to Ambler notation<sup>65</sup> and correspond to residue numbers 43-307 of BlaC Uniprot entry P9WKD3-1, 29-291 of CTX-M-14 Uniprot entry Q9L5C7, 25-293 of KPC-2 Uniprot entry Q9F663, 28-292 of NMC-A Uniprot entry P52663, and 24-286 of TEM-1 Uniprot entry P62593. The purple shading indicates the degree of sequence identity. For in-cell studies, these sequences are preceded by a Tat-signal sequence, for *in vitro* studies an N-terminal TEV cleavable HIS-tag was added.<sup>172</sup>

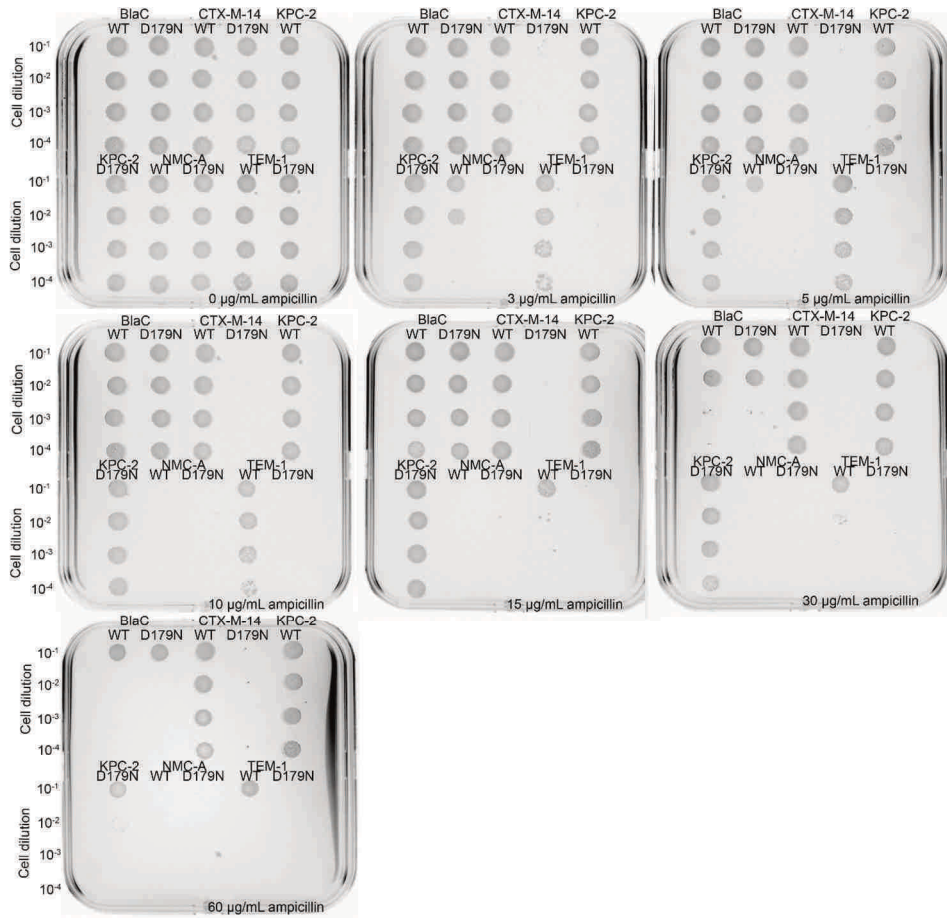


**Figure S3.7.** Activity against ampicillin of five class A β-lactamases. Cultures of *E. coli* expressing genes of the wild type or D179N variants of β-lactamases BlaC, CTX-M-14, KPC-2, NMC-A or TEM-1 were spotted in increasing dilution on plates containing various concentration of ampicillin.

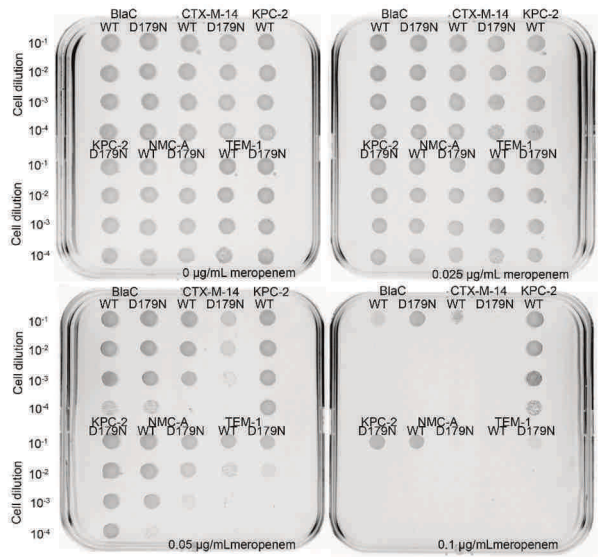


**Figure S3.8.** Activity against meropenem of five class A  $\beta$ -lactamases. Cultures of *E. coli* expressing genes of the wild type or D179N variants of  $\beta$ -lactamases BlaC, CTX-M-14, KPC-2, NMC-A or TEM-1 were spotted in increasing dilution on plates containing various concentration of meropenem. The plate without ampicillin in Figure S3.7.



**Figure S3.9.** Activity against carbenicillin of five class A  $\beta$ -lactamases. Cultures of *E. coli* expressing genes of the wild type or D179N variants of  $\beta$ -lactamases BlaC, CTX-M-14, KPC-2, NMC-A or TEM-1 were spotted in increasing dilution on plates containing various concentration of carbenicillin.

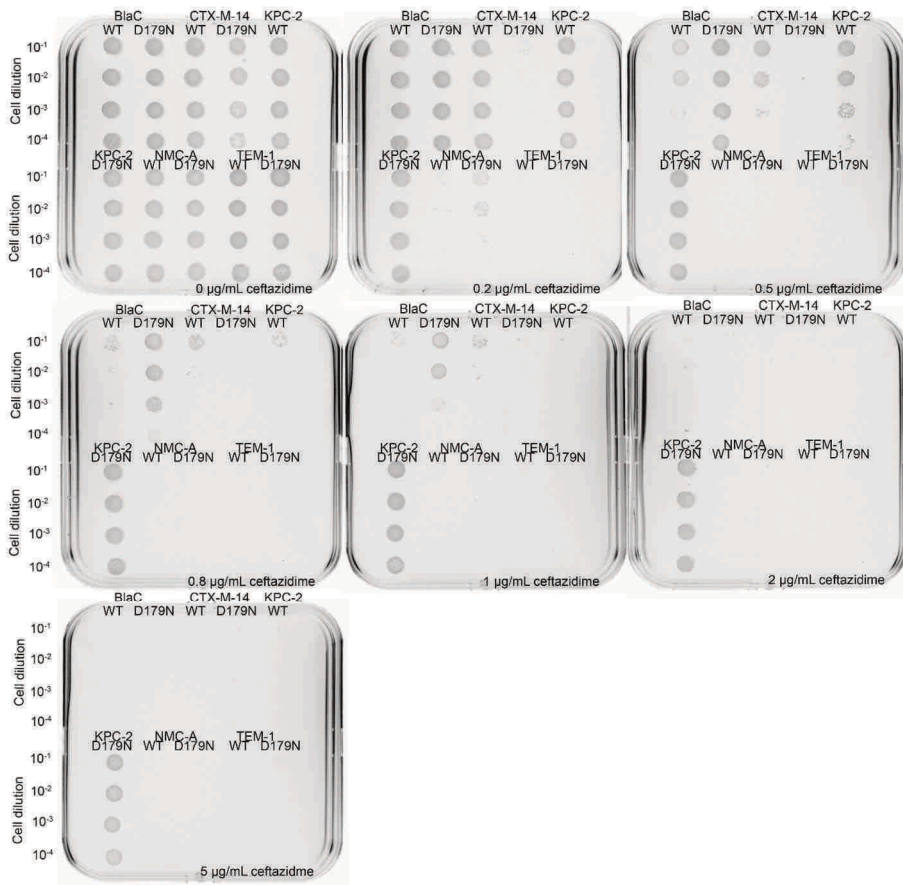


**Figure S3.10.** Activity against ceftazidime of five class A  $\beta$ -lactamases. Cultures of *E. coli* expressing genes of the wild type or D179N variants of  $\beta$ -lactamases BlaC, CTX-M-14, KPC-2, NMC-A or TEM-1 were spotted in increasing dilution on plates containing various concentration of ceftazidime.

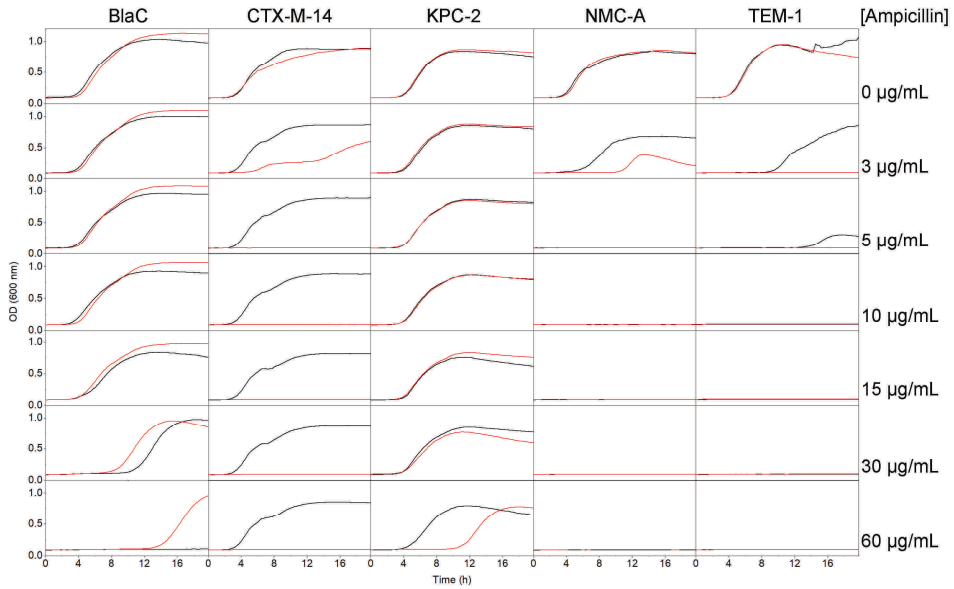


**Figure S3.11.** Activity against ampicillin of five class A  $\beta$ -lactamases. Cultures of *E. coli* expressing genes of the wild type (black) or D179N variants (red) of  $\beta$ -lactamases BlaC, CTX-M-14, KPC-2, NMC-A or TEM-1 were grown in liquid cultures for 20 hours. The OD<sub>600</sub> is plotted as a function of time.

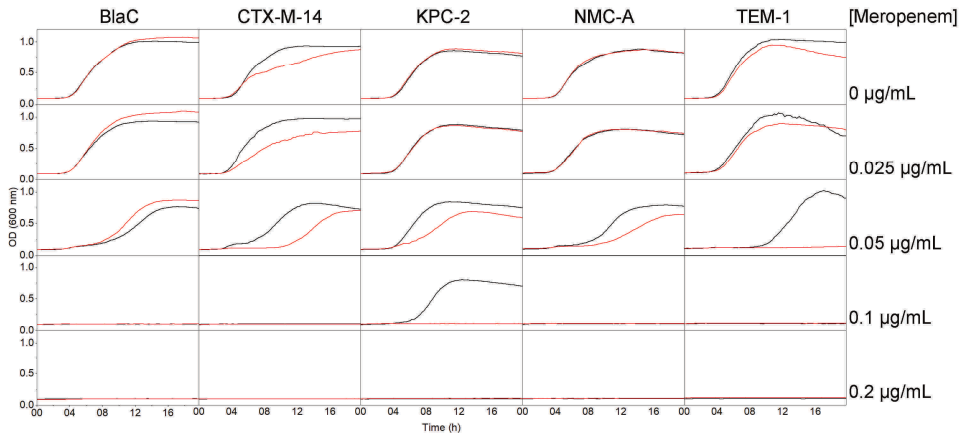


**Figure S3.12.** Activity against meropenem of five class A  $\beta$ -lactamases. Cultures of *E. coli* expressing genes of the wild type (red) or D179N variants (black) of  $\beta$ -lactamases BlaC, CTX-M-14, KPC-2, NMC-A or TEM-1 were grown in liquid cultures for 20 hours. The OD<sub>600</sub> is plotted as a function of time.

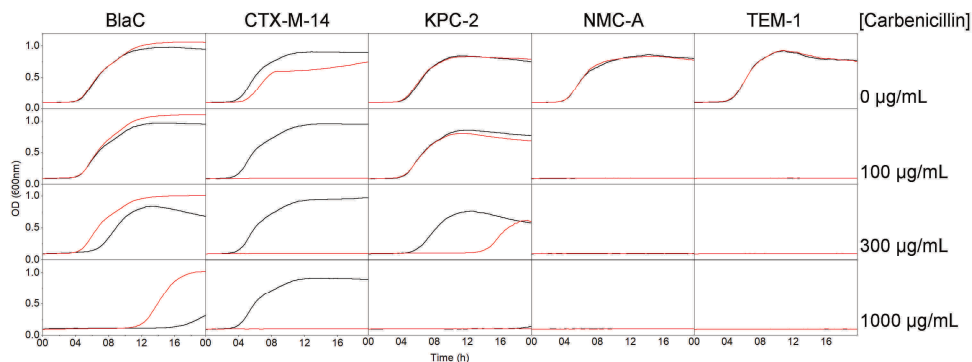


**Figure S3.13.** Activity against carbenicillin of five class A  $\beta$ -lactamases. Cultures of *E. coli* expressing genes of the wild type (black) or D179N variants (red) of  $\beta$ -lactamases BlaC, CTX-M-14, KPC-2, NMC-A or TEM-1 were grown in liquid cultures for 20 hours. The OD<sub>600</sub> is plotted as a function of time.

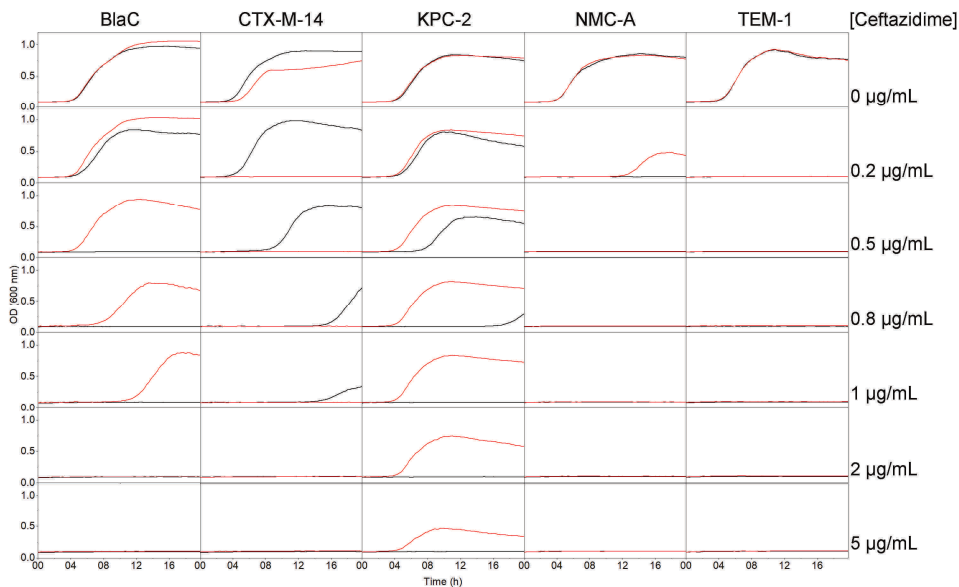


**Figure S3.14.** Activity against ceftazidime of five class A  $\beta$ -lactamases. Cultures of *E. coli* expressing genes of the wild type (black) or D179N variants (red) of  $\beta$ -lactamases BlaC, CTX-M-14, KPC-2, NMC-A or TEM-1 were grown in liquid cultures for 20 hours. The OD<sub>600</sub> is plotted as a function of time. Data for 0  $\mu\text{g mL}^{-1}$  ceftazidime is the same as for 0  $\mu\text{g mL}^{-1}$  carbenicillin in Figure S3.13.